

Using Advanced Molecular Profiling to Identify the Origin of and Tailor Treatment for an Intracranial Mass of Unknown Primary

Francisco Martinez, MD¹; Eric Brucks, MD¹; Janelle Otsuji, MD²; Haseeb Mehnoor, MS³; Hina Arif-Tiwari, MD⁴; Hani M. Babiker, MD⁵; and Alejandro Recio-Boiles, MD⁵

CASE DESCRIPTION

A 53-year-old White gentleman, with no significant past medical history other than active tobacco use, woke up with a sudden onset of double vision and severe frontal headaches (Fig 1). In the past 4 weeks, his vision progressively worsened and he developed left facial numbness. Because of deterioration of his symptoms, the patient was seen by ophthalmology and found to have a left lateral gaze. His magnetic resonance imaging showed a 34 mm × 17 mm clival mass with extension into the prepontine cistern, both Meckel's caves, both sphenoid sinuses, and both petrous apices (Fig 3, Row 1). Additionally, the mass showed encasement of the left cavernous internal carotid artery. The combination of worsening vision and mass location led to the differential diagnosis of macroadenoma, neural primary malignancy, or metastatic carcinoma of unknown primary.

The patient was seen by ear nose and throat specialists. A nasal endoscopy was performed, and he was subsequently referred to neurosurgery. The patient underwent a transsphenoidal tumor resection under their care. Pathology from the clival mass showed nests of highly atypical cells with focal glandular and cribriform architecture. Immunohistochemistry demonstrated that the clival mass cells were diffusely positive for pankeratin (OSCAR). The cells also exhibited patchy positivity for cytokeratin 7 (CK7), and the mucicarmine stain showed focal extracellular mucin. The clival mass cells had negative markers for p40, cytokeratin 5 (CK5), thyroid transcription factor 1, Napsin-A, caudal-type homeobox transcription factor 2, cytokeratin 20 (CK20), sry-related hmg-box gene 10 (SOX10), prostate-specific antigen (PSA), prostatic acid phosphatase (PSAP), paired box 8 (PAX8), and GATA-binding protein 3 (GATA3). These findings were indicative of a high-grade adenocarcinoma, but the immunophenotype was not specific for primary disease (Fig 2, top row). Informed consent for the use of the radiology images was obtained from the patient presented.

The day after the clival mass resection, the patient underwent an inpatient computed tomography of his

neck, chest, abdomen, and pelvis. The scan showed numerous hepatic, pulmonary, osseous, and nodal metastatic lesions, which seemed suspicious. It also showed a benign incidental follicular thyroid mass (later biopsy-proven). After a 3-day hospital admission, a subsequent outpatient positron emission tomography scan demonstrated fluorodeoxyglucose avidity of the residual clival mass (Fig 3). In addition, it also exhibited probable metastatic lesions in the lungs, liver, bone, and lymph nodes. At this stage, definitively discerning the primary site of the malignancy remained a challenge. The team decided to proceed with palliative radiation therapy for symptom control with a combined radiation dose of 37.5 Gy across 14 fractions directed to the clival mass.

A thorough history, physical examination, and laboratory workup were completed per National Comprehensive Cancer Network (NCCN) guidelines for the management of cancers of unknown primary. Despite presenting symptoms and physical findings, the patient denied all pertinent cancer-associated complaints (eg, weight loss, night sweats, etc) and the physical examination did not reveal any pertinent positive findings (eg, palpable adenopathy). Initial serum tumor markers revealed elevated levels for alpha-fetoprotein at 218 ng/mL (normal < 8.7 ng/mL), carbohydrate antigen 19-9 (CA 19-9) at 49 U/mL (normal < 35 U/ml), and chromogranin A at 1,120 ng/mL (normal < 140 ng/ml). The workup also showed normal levels of carcinoembryonic antigen and PSA. Additionally, his hemoglobin, AST, ALT, creatine, and electrolytes including calcium were also normal. His family history was negative for any malignancies. Relevant social history included tobacco use (30 pack-year), occasional alcohol use, having worked as a retail store manager, and having no travel history outside of the continental United States. Further history did not reveal any exposure to liver flukes, schistosomiasis, a history of sexually transmitted diseases, or prior blood transfusions. For comprehensive evaluation, the original surgically resected clival biopsy sample underwent additional tumor profile assays accompanied by a plasma liquid biopsy. The following

Author affiliations and support information (if applicable) appear at the end of this article.

Accepted on April 28, 2021 and published at [ascopubs.org/journal/po](https://doi.org/10.1200/P0.20.00243) on June 10, 2021; DOI <https://doi.org/10.1200/P0.20.00243>

Creative Commons Attribution Non-Commercial No Derivatives 4.0 License 

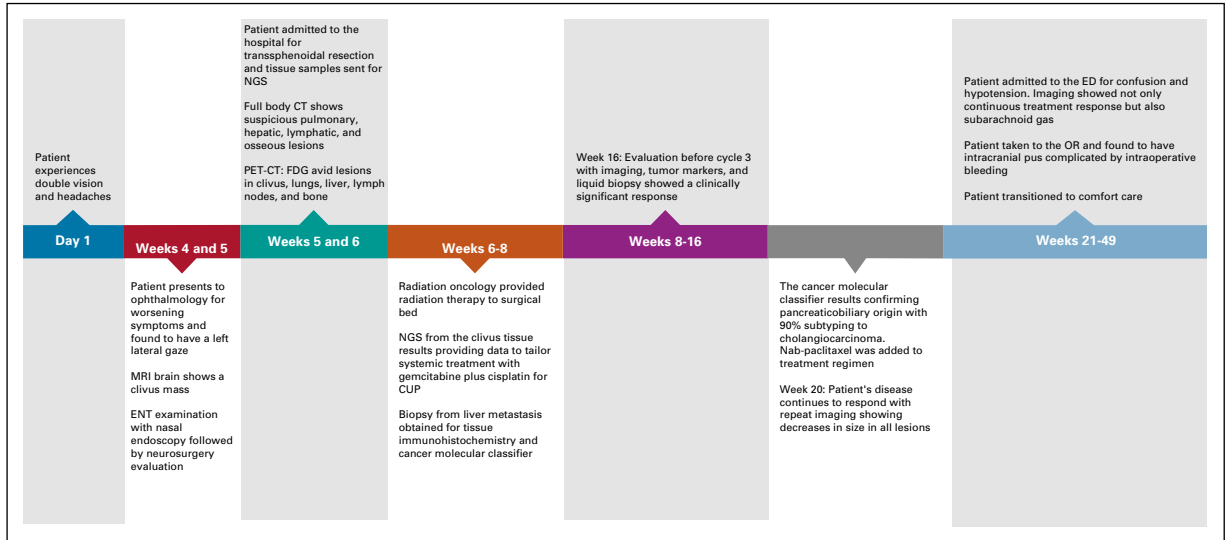


FIG 1. Timeline. CT, computed tomography; CUP, cancer of unknown primary; ED, emergency department; ENT, ear, nose, and throat; FDG, fluorodeoxyglucose; MRI, magnetic resonance imaging; NGS, next-generation sequencing; OR, operating room; PET, positron emission tomography.

week, a core needle liver biopsy was performed by interventional radiology. A tissue molecular cancer classifier was planned for this sample. With pathologic analysis pending, the working diagnosis was either primary pituitary carcinoma or metastatic carcinoma to the pituitary. The patient's systemic therapeutic management was uniquely tailored because of a lack of standard of care for this exceedingly rare clinical presentation. Management was accomplished by using data available from a next-gen sequencing profile

(CARIS) conducted on the original clival mass, and the patient was started on treatment with cisplatin 25 mg/m² combined with gemcitabine 1,000 mg/m² with future consideration of nab-paclitaxel 100 mg/m² were administered on days 1 and 8 of 21-day cycles.

Surprisingly, a molecular cancer classifier (CancerTYPE ID) from the liver biopsy pointed to a pancreaticobiliary origin with a 90% probability subtype match to cholangiocarcinoma, not pituitary carcinoma. Further attempts to determine

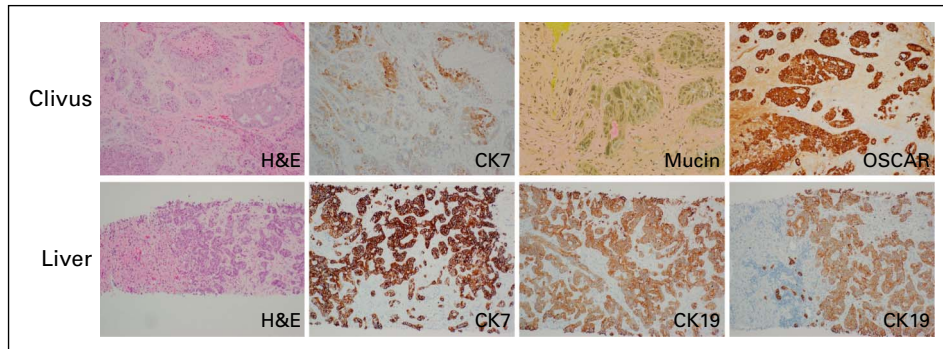


FIG 2. Pathology. Top row: Clivus mass stains at 10 × magnification. H&E of the primary mass showing infiltrative nests with glands with focal necrosis and cribriform architecture. CK7 by immunohistochemistry showing focal expression within the tumor cells (CK20-negative). Special stain mucicarmine showing focal positivity for extracellular mucin and diffuse positivity for CK OSCAR. Clivus mass was negative for p40 (squamous cell), CK5, TTF-1, Napsin-A, CDX2, SOX10, PSA/PSAP, PAX8, and GATA3. Bottom row showing liver biopsy stains at 10 × magnification. H&E needle core biopsy of the liver mass showing infiltrative highly atypical cells forming abortive acini and adjacent uninvolved liver to the left. CK7/CK19 stain showing strong expression within the tumor cells. Liver biopsy was negative for TTF-1, Napsin-A, CK20, and GATA3. In conjunction with the clivus mass resection, these findings are supportive of high-grade adenocarcinoma suggestive of pancreaticobiliary origin. CK, cytokeratin; GATA3, GATA-binding protein 3; H&E, hematoxylin and eosin; PAX8, paired-box 8; PSA, prostate specific antigen; PSAP, prostatic acid phosphatase; SOX10, sry-related hmg-box gene 10; TTF-1, thyroid transcription factor 1.

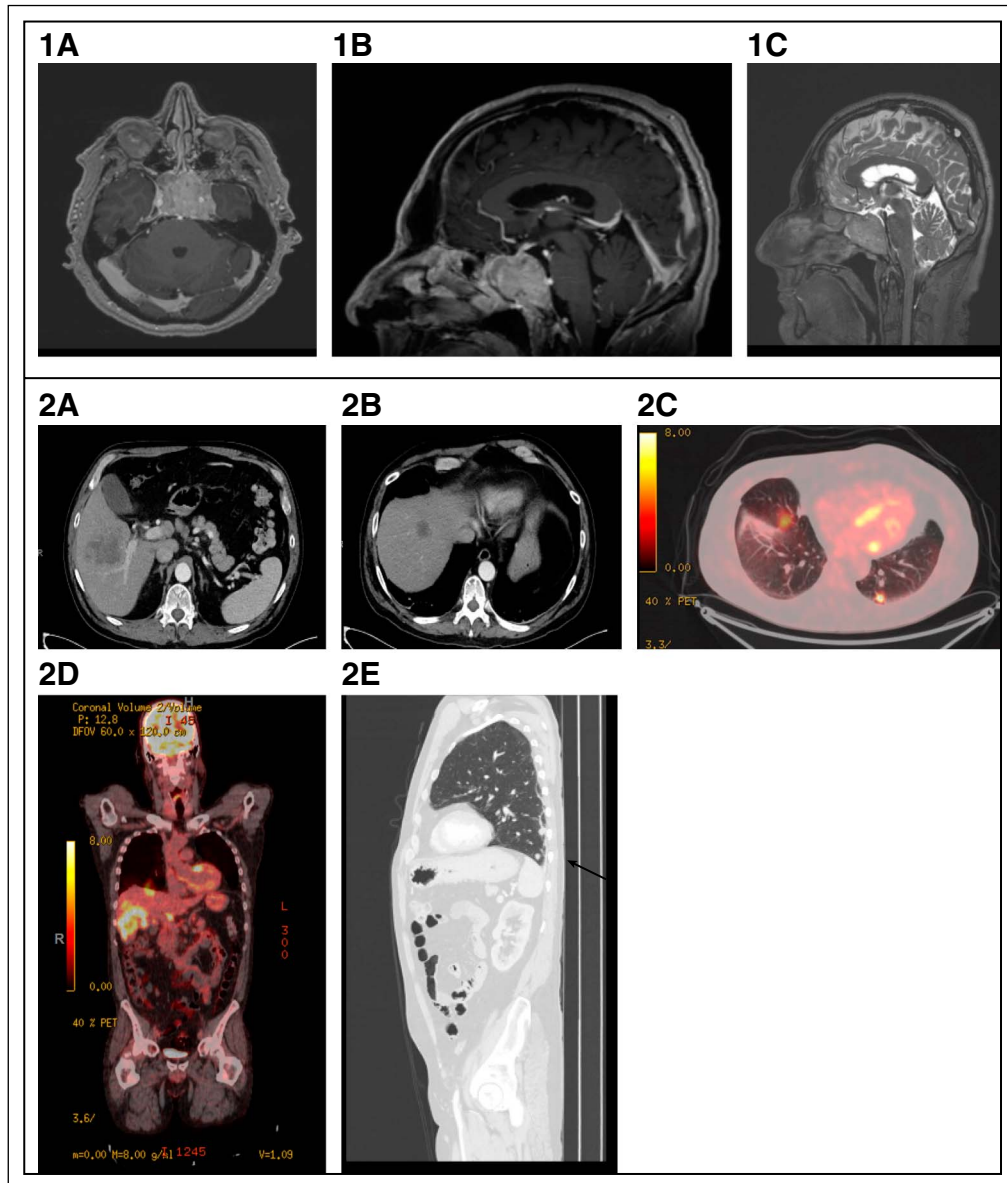


FIG 3. Radiology. 1. Expansile infiltrative clival tumor is seen on (A) sagittal T2-weighted images, which uniformly enhances on (B) sagittal MPRAGE postcontrast image. The mass extends anteriorly into both sphenoid sinuses and laterally encases the adjacent internal carotid artery, which remains patent, seen on (C) axial and coronal MPRAGE postcontrast images. In light of the aggressive infiltrative appearance, imaging differential of invasive pituitary macroadenoma or metastasis was considered. 2. Five weeks after presentation: (A and B, arrows) Multiple, bilobar liver metastases are seen, (B, arrowhead) in addition to upper abdominal lymphadenopathy by contrast-enhanced CT of the chest abdomen and pelvis. (C, arrows) Pulmonary metastasis was present in the left lung (C, D, E). PET-CT examination showed avid fluorodeoxyglucose uptake in the pulmonary and hepatic metastasis and malignant lymphadenopathy. 3. (A) Post-treatment sagittal MPRAGE MR examination reveals a reduction in the size of the clival tumor (B, C, D). Contrast-enhanced CT of the abdomen also shows reduced liver metastasis and malignant lymphadenopathy. CT, computed tomography; MR, magnetic resonance; PET, positron emission tomography.

the primary site by immunohistochemistry (IHC) stains were made on the liver biopsy, including mucicarmine (Mucin), Hepatocyte Paraffin 1 (Heppar1), CK5, CK7, CK20, p40, thyroid transcription factor 1, Napsin-A, CDX2, SOX10, PSA,

PSAP, PAX8, and GATA3 (Fig 2, bottom row). The biopsy of the liver lesion showed similar morphology with tumor cells positive for CK7 and CK19. In conjunction, the analysis favored the same primary for both the clival mass and liver

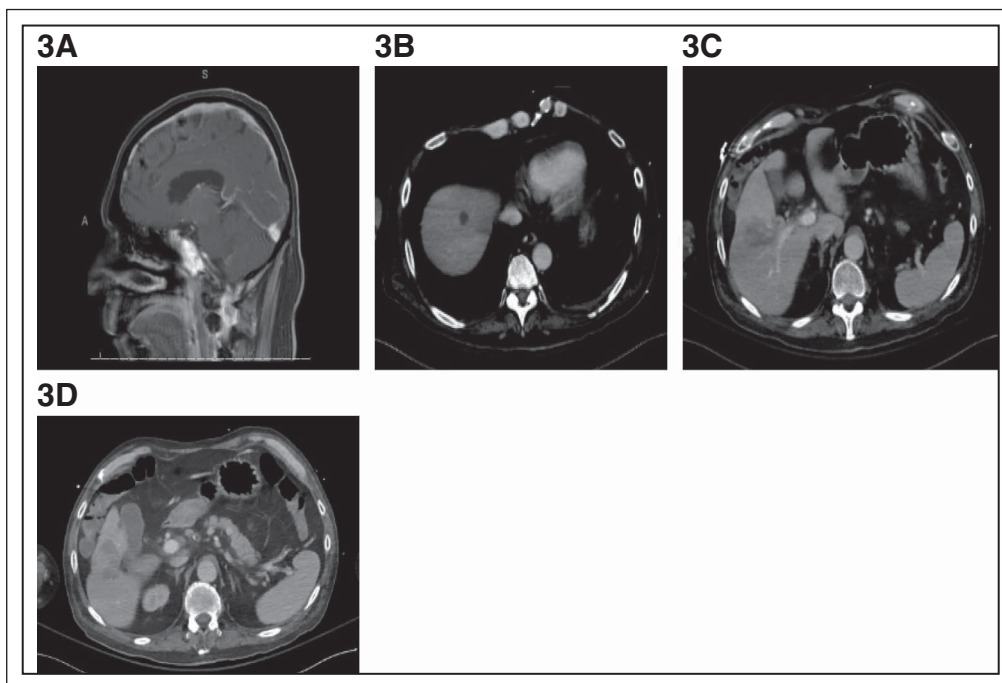


FIG 3. (Continued).

lesions. Analysis supported the diagnosis of high-grade adenocarcinoma suggestive of cholangiocarcinoma.

Eight weeks after initiation of two well-tolerated full-dose treatment cycles of cisplatin and gemcitabine, the patient was reimaged. Imaging showed an interval decrease in size by 48% for liver lesions, 59% for lymph nodes, 33% for the lung nodules, and 27% for clival mass according to the RECIST 1.1 guidelines (Fig 3). A repeat CA 19-9 test showed a 30% reduction to below normal levels. The patient at this point was enrolled in a research study looking at correlating CA 19-9 with liquid biopsies. A subsequent repeat liquid biopsy analysis (Guardant360) was performed and did not detect the previously reported driver mutations at baseline. This result suggested a response to the regimen (Table 1). Nab-paclitaxel was added to the cisplatin-gemcitabine regimen on the basis of recent positive pancreaticobiliary phase II trials.^{1,2} Repeat imaging at 12 weeks of treatment showed a continuous response with a decrease in size (measured per RECIST 1.1 guidelines) of the intrahepatic lesions by 53% and clival mass by 37% from baseline (Fig 2).

During the ninth cycle, the patient was admitted to the emergency department for hypotension after his knees buckled when walking down the hall at home. Shortly after, he became altered and confused. The patient had an emergent head computed tomography, which was negative for acute bleed. The scan showed no evidence of new metastatic disease and most notably significantly reduced volume of the previously described clival mass. These findings were corroborated by continuing mild reduction of

the overall tumor burden on body imaging. Despite those positives, the scan revealed interval development of diffuse subarachnoid gas with additional extra-axial gas along the left anterior frontal lobe. The patient underwent neurosurgery in response, which encountered gross pus in the sphenoid sinus region. Complication later arose from bleeding of the basilar and vertebral arteries. At first glance, the cause seemed because of a bacterial infection, but further inspection uncovered that it was a result of the tumor dissolution. The tumor had previously replaced the normal epithelium and acted as the CNS/CSF barrier for the arteries. With the tumor dissolved, the weakened structure resulted in the bleeding. After the infection and bleeding were controlled, the patient was placed on a ventilator and transferred to the intensive care unit. He showed no neurologic clinical recovery the subsequent week, and the goals of care discussion was conducted with the family. The patient ultimately passed in the following days from cardiac arrest not attributed directly to cancer progression.

The patient provided informed consent allowing discussion of his case and inclusion of pertinent images. This investigation was performed after approval by a local Human Investigations Committee and in accordance with guidelines approved by the Department of Health and Human Services.

MOLECULAR TUMOR BOARD EVIDENCE-BASED DECISION

Given that cross-sectional imaging and pathology failed to produce an identifiable primary origin for the tumor, we elected to further categorize the mass by using clinically available comprehensive tumor profilers. Cancer of

TABLE 1. List of CARIS and Guardant 360 Mutations

Next-Gen Sequencing Profile (CARIS)	Finding
Microsatellite instability	Stable
Tumor mutational load	Low 4 mutations/Mb
Mismatch repair status	Proficient
MLH1 IHC-positive	2+, 90%
MSH2 IHC-positive	2+, 90%
MSH6 IHC-positive	1+, 90%
PMS2 IHC-positive	1+, 50%
PD-L1 IHC-positive	2+, 5%
Mutated and pathogenic	ATM NGS Exon 56 p.R2748fs BAP1 NGS Exon 16 p.L662fs
NTRK1, 2, and 3 fusions	Not detected
BRAF NGS mutation	Not detected
BRCA1 NGS mutation	Not detected
BRCA2 NGS mutation	Not detected
EGFR NGS mutation	Not detected
KRAS NGS mutation	Not detected
NRAS NGS mutation	Not detected
ERBB2 (HER2/Neu) NGS amplification	Not detected
ERCC1 IHC-negative I	0, 100%
RRM1 IHC-negative I	2+, 5%
TOPO1 IHC-negative I	2+, 20%
TS IHC-negative I	1+, 5%
Plasma Liquid Biopsy Analysis (Guardant 360)	Finding
Pretreatment (baseline)	Low 2.2%
BRAF amplification	
CDK6 amplification	Low 2.2%
MET T67N	Low 0.2%
IDH1-2 mutation	Not detected
FGFR1-4 fusion	Not detected
PIK3CA mutation	Not detected
MET mutation	Not detected
ROS1 mutation	Not detected
CDK6 mutation	Not detected
Post-treatment (8 weeks or 2 cycles)	
BRAF amplification	Not detected
CDK6 amplification	Not detected
MET T67N	Not detected
IDH1-2 mutation	Not detected
FGFR1-4 fusion	Not detected
PIK3CA mutation	Not detected
MET mutation	Not detected
ROS1 mutation	Not detected
CDK6 mutation	Not detected
CDK6 amplification	Not detected
MET T67N	Not detected

NOTE. Guardant samples were sent pre- and post-treatment June 07, 2018-September 18, 2018.

Abbreviations: IHC, immunohistochemistry; NGS, next-generation sequencing.

unknown primary (CUP) can be divided into multiple favorable subcategories, which benefit from specifically tailored treatment regimens.³ According to NCCN guidelines, the patient's clinical presentation best matched adenocarcinoma with numerous sites of involvement and male with negative PSA (OCC-6). By the European Society for Medical Oncology guidelines, the patient did not have a distinct subset of CUP on the basis of his clinical and pathologic criteria. More than 80% of CUPs do not fall into these subcategories. In patients harboring these malignancies, an empiric palliative therapy of docetaxel or paclitaxel, used in parallel with gemcitabine (combined with either carboplatin or irinotecan), is often the preferred regimen used for poor-risk patients with a grim prognosis. The presence of intracranial disease provoked us to tailor a better regimen, as there are limited data on this subcategory of CUP.

The initial results identified multiple mutations that allowed us to guide our clinical suspicion of the tumor origin and tailor therapy in a mutation-specific manner (CARIS Molecular Intelligence Tumor Profiling, Table 1). The molecular profile used IHC, in situ hybridization, next-generation sequencing (NGS), Sanger sequencing, Pyro sequencing (PyroSeq), and fragment analysis (FA/Frag. Analysis). In our sample, microsatellite instability and 592 individual genes were tested via NGS and nine were tested via IHC. The studies returned with BRCA1-associated protein 1 (BAP1) Exon 16 mutation at a frequency of 52% and an indeterminate result on the loss of AT-Rich Interacting Domain-containing protein 1A (ARID1A). This indicated early on that the primary may be intracholangiocarcinoma.⁴⁻⁷ BAP1 and ARID1A's main differential diagnoses are urothelial, renal cell carcinoma, melanoma, and mesothelioma. These were considered less likely without the clinical presentation, missing primary organ lesion, nonsupportive IHC, and further exclusion supported by the molecular cancer classifier. The BAP1 Exon 16 and ataxia telangiectasia-mutated Exon 56 present with a frequency of 68%, in genes playing roles in repairing damaged DNA. This implied that the malignancy was likely to respond to a platinum-based treatment regimen.⁸ Ribonucleotide reductase M1, needed for polymerization and repair of DNA, was present but with only a 5% IHC staining. This suggested that there may be some benefit from the gemcitabine addition to the therapy regimen.^{9,10} Tubulin beta-3 was found to be positive with a 70% staining by IHC, which is known to be a potential target for taxanes, including nab-paclitaxel.¹¹⁻¹³ Other common molecular targets associated with IHC, such as isocitrate dehydrogenase 1, multidrug resistance mutation, and fibroblast growth factor receptor, were negative in the tumor profile. Unfortunately, this meant that they could not be used to tailor first-line treatment (Table 1). Potentially, if other first-line treatment failure occurred, the patient could be considered for a clinical trial that is enrolling patients with ataxia telangiectasia-mutated mutations. They could also be treated with poly (ADP-ribose) polymerase or histone

deacetylase inhibitors. We decided to proceed with cisplatin-gemcitabine regimen with nab-paclitaxel, now that we knew the likely identity of the malignancy and its molecular characteristics. This regimen is well-defined for pancreaticobiliary carcinomas. It has a median progression-free survival of 11.8 months and an overall survival of 19.2 months^{1,2} rather than an empiric two-drug regimen, which has docetaxel and carboplatin with a median of overall survival of 5 months on visceral metastasis.¹⁴

The radiologic findings, the serum tumor markers, and NGS were suggestive of a pancreaticobiliary origin. Furthermore, the liver biopsy stains and the prior clivus mass had similar morphology. Together, these findings were supportive of high-grade adenocarcinoma suggestive of pancreaticobiliary origin; however, other primaries could not be excluded (Fig 2). Ultimately, the metastatic liver lesion was classified using the validated gene expression test, CancerTYPE ID, which uses real-time polymerase chain reaction to amplify 92 genes to classify a tumor on the basis of a database of tumor types and subtypes. The tumor was identified as most likely pancreaticobiliary in origin with a 90% likelihood of cholangiocarcinoma.

A liquid biopsy (Guardant360) tested 74 genes for point mutations and deletion variants, 18 genes for amplification, and six genes for fusions. The patient was enrolled in a

research study assessing liquid biopsies, which allowed a repeat liquid biopsy testing and analysis post-treatment. The Guardant360 test provided detectable baseline amplifications of BRAF, CDK6, and MET T67N at 2.2%, 2.2%, and 0.2%, respectively. These are considered useful biomarkers to predict treatment response, and after three cycles, these amplifications were found undetectable across all three genes. At the same time, there was a partial response in serum tumor markers and measurable disease burden by RECIST 1.1 criteria over the same interval. Although repeat liquid biopsy analysis is not currently standard of care as this tool becomes more affordable and available, it may be more feasible to use it as an additional tool to monitor response.

The patient ultimately survived 12 months without progression after the initial lesion was found. This timeframe significantly exceeds the expected survival of intracranial metastatic cholangiocarcinoma. Although the patient died of non-cancer complications after having achieved a great response, this case demonstrates the benefit and utility of comprehensive molecular profiling in both identifying site of origin and tailoring therapy in cases of unknown primary as recommended by NCCN or by participation in clinical trials (CUPISCO ClinicalTrials.gov identifier: NCT03498521).¹⁵

AFFILIATIONS

¹Department of Medicine, University of Arizona, Tucson, AZ

²Department of Pathology, University of Arizona, Tucson, AZ

³College of Medicine, University of Arizona, Tucson, AZ

⁴Department of Medical Imaging, University of Arizona, Tucson, AZ

⁵Division of Hematology-Oncology, Department of Medicine, University of Arizona Cancer Center, University of Arizona, Tucson, AZ

CORRESPONDING AUTHOR

Francisco Martinez, MD, Internal Medicine Residency Program, Department of Medicine, University of Arizona College of Medicine—Tucson, 1501 N. Campbell Ave, Tucson, AZ 85724; e-mail: fmartinez@deptofmed.arizona.edu.

SUPPORT

Supported by 2P30 CA023074 supplement of the Cancer Center Support Grant from the NCI/NIH to the University of Arizona Cancer Center.

AUTHOR CONTRIBUTIONS

Conception and design: Francisco Martinez, Haseeb Mehnoor, Hani M. Babiker, Alejandro Recio-Boiles

Administrative support: Hani M. Babiker, Alejandro Recio-Boiles

Provision of study materials or patients: Hani M. Babiker, Alejandro Recio-Boiles

Collection and assembly of data: Francisco Martinez, Haseeb Mehnoor, Hina Arif-Tiwari, Hani M. Babiker, Alejandro Recio-Boiles

Data analysis and interpretation: Francisco Martinez, Eric Brucks, Janelle Otsuji, Hina Arif-Tiwari, Hani M. Babiker, Alejandro Recio-Boiles

Manuscript writing: All authors

Final approval of manuscript: All authors

Accountable for all aspects of the work: All authors

AUTHORS' DISCLOSURES OF POTENTIAL CONFLICTS OF INTEREST

The following represents disclosure information provided by the authors of this manuscript. All relationships are considered compensated unless otherwise noted. Relationships are self-held unless noted. I = Immediate Family Member, Inst = My Institution. Relationships may not relate to the subject matter of this manuscript. For more information about ASCO's conflict of interest policy, please refer to www.asco.org/rwc or ascopubs.org/po/author-center.

Open Payments is a public database containing information reported by companies about payments made to US-licensed physicians ([Open Payments](http://OpenPayments)).

Hani M. Babiker

Consulting or Advisory Role: Endocyte, Celgene, Idera, Myovant Sciences

Speakers' Bureau: Guardant Health

No other potential conflicts of interest were reported.

ACKNOWLEDGMENT

We thank Brittany Madrigal, clinical editor.

REFERENCES

1. Jameson GS, Borazanci EH, Babiker HM, et al: A phase Ib/II pilot trial with nab-paclitaxel plus gemcitabine plus cisplatin in patients (pts) with stage IV pancreatic cancer. *J Clin Oncol* 35, 2017 (suppl; abstr 341)
2. Shroff RT, Javle MM, Xiao L, et al: Gemcitabine, cisplatin, and nab-paclitaxel for the treatment of advanced biliary tract cancers: A phase 2 clinical trial. *JAMA Oncol* 5:824-830, 2019
3. National Comprehensive Cancer Network: NCCN Guidelines Version 3.2020 Ocuult Primary, 2020. https://www.nccn.org/professionals/physician_gls/pdf/ocult.pdf
4. Andrici J, Goeppert B, Sioson L, et al: Loss of BAP1 expression occurs frequently in intrahepatic cholangiocarcinoma. *Medicine* 95:e2491, 2016
5. Jiao Y, Pawlik TM, Anders RA, et al: Exome sequencing identifies frequent inactivating mutations in BAP1, ARID1A and PBRM1 in intrahepatic cholangiocarcinomas. *Nat Genet* 45:1470, 2013
6. Zou S, Li J, Zhou H, et al: Mutational landscape of intrahepatic cholangiocarcinoma. *Nat Commun* 5:5696, 2014
7. Ross JS, Wang K, Gay L, et al: New routes to targeted therapy of intrahepatic cholangiocarcinomas revealed by next-generation sequencing. *Oncologist* 19:235-242, 2014
8. Golan T, Raitses-Gurevich M, Kelley RK, et al: Overall survival and clinical characteristics of BRCA-associated cholangiocarcinoma: A multicenter retrospective study. *Oncologist* 22:804-810, 2017
9. Gong W, Zhang X, Wu J, et al: RRM1 expression and clinical outcome of gemcitabine-containing chemotherapy for advanced non-small-cell lung cancer: A meta-analysis. *Lung Cancer* 75:374-380, 2012
10. Kwon WS, Rha SY, Choi YH, et al: Ribonucleotide reductase M1 (RRM1) 2464G>A polymorphism shows an association with gemcitabine chemosensitivity in cancer cell lines. *Pharmacogenet Genomics* 16:429-438, 2006
11. Ploussard G, Terry S, Maillé P, et al: Class III β -tubulin expression predicts prostate tumor aggressiveness and patient response to docetaxel-based chemotherapy. *Cancer Res* 70:9253-9264, 2010
12. Zhang HL, Ruan L, Zheng LM, et al: Association between class III β -tubulin expression and response to paclitaxel/vinorelbine-based chemotherapy for non-small cell lung cancer: A meta-analysis. *Lung Cancer* 77:9-15, 2012
13. Seve P, Mackey J, Isaac S, et al: Class III β -tubulin expression in tumor cells predicts response and outcome in patients with non-small cell lung cancer receiving paclitaxel. *Mol Cancer Ther* 4:2001-2007, 2005
14. Pentheroudakis G, Briasoulis E, Kalofonos HP, et al: Docetaxel and carboplatin combination chemotherapy as outpatient palliative therapy in carcinoma of unknown primary: A multicentre Hellenic Cooperative Oncology Group phase II study. *Acta Oncol* 47:1148-1155, 2008
15. Rodon J, Soria J, Berger R, et al: Genomic and transcriptomic profiling expands precision cancer medicine: The WINTHER trial. *Nat Med* 25:751-758, 2019

